PRAMANA
— journal of
physics

© Indian Academy of Sciences

Vol. 86, No. 4
April 2016
pp. 723–736

A physics-based potential and electric field model of a nanoscale rectangular high-K gate dielectric HEMT

B DAS, R GOSWAMI and B BHOWMICK*

Electronics and Communication Engineering Department, National Institute of Technology, Silchar 788 010, India

*Corresponding author. E-mail: brindabhowmick@gmail.com

MS received 15 October 2014; revised 19 February 2015; accepted 11 March 2015

DOI: 10.1007/s12043-015-1100-y; ***e*Publication:** 17 November 2015

Abstract. In this paper, we have developed a physics-based model for surface potential, channel potential, electric field and drain current for AlGaN/GaN high electron mobility transistor with high-K gate dielectric using two-dimensional Poisson equation under full depletion approximation with the inclusion of effect of polarization charges. The accuracy of the model has been verified and is found to be in good agreement with the simulated results.

Keywords. AlGaN/GaN; HEMT; surface potential; channel potential; electric field.

PACS Nos 02.30.Jr; 05.60.Cd; 77.55.D−; 02.60.Cb

1. Introduction

With the recent advancement in semiconductor technology, HEMTs have emerged as the most suitable candidates for radio frequency and microwave power because AlGaN/GaN HEMTs provide large band gap, high electron velocity and high thermal stability [1–3].

While AlGaN/GaN HEMTs are fairly mature, gate leakage current is the major drawback. Gate leakage current can introduce additional noise source [4] and reliability problem [5]. Therefore gate dielectric is introduced to reduce gate leakage current [6–8].

Various models are available for AlGaN/GaN HEMT devices based on numerical calculations, semiempirical model, simplifying approximations [9–11] and device physics [12–18], but mathematical model for AlGaN/GaN HEMTs with gate dielectric has not yet been developed. However, Shenghui *et al* [19] proposed an analytical charge control model for AlGaN/GaN MIS-HEMTs including undepleted barrier layer, which successfully modelled transfer characteristics. However, electric field, channel, surface potential and current were not modelled. This paper presents, for the first time, a physics-based model for potential and electric field in a nanoscale rectangular high-K dielectric HEMT using 2D Poisson's equation.

2. Device structure

In this work, along with AlGaN cap layer [20], gate dielectric has been introduced under rectangular metal gate, extended from source to drain.

The 2D schematic of HEMT is shown in figure 1. It consists of SiC substrate, an AlN nucleation layer between undoped GaN and SiC, an n-doped AlGaN barrier layer of thickness $d_a = 25$ nm and doping concentration $N_d = 4 \times 10^{18}$ cm^{-3}, an undoped AlGaN cap layer of thickness $d_c = 5$ nm, an undoped AlGaN layer of thickness $d_s = 5$ nm between GaN and AlGaN and hafnium oxide (HfO_2) as high-K gate dielectric having thickness $t_{ox} = 10$ nm and permittivity $\varepsilon_{ox} = 22$ under the metal gate. Gate metal used is tantalum nitride (work function = 4.8 eV). Source and drain regions are modelled as heavily doped regions with concentration $N_{d+} = 10^{22}$ cm^{-3}. Here, gate to drain and source spacing is kept constant at $L_{GD} = L_{GS} = 30$ nm. The total length of the device is 240 nm. At $y = 0$, it is bounded by interface with the gate dielectric and on the lower side, it is bounded by the heterointerface at $y = d = d_c + d_a + d_s$.

3. Model formulation

To develop a model, we consider three regions in the channel where Regions I and III consist of regions which are not under gate metal and Region II consists of region under gate metal (marked in figure 1). The analytical model for the proposed device has been derived by solving 2D Poisson's equation in the three regions respectively. While deriving the model for the proposed device, we have assumed uniform impurity concentration and considered that the regions are fully depleted (table 1).

The 2D Poisson equation is given by

$$\frac{d^2\phi(x,y)}{dx^2} + \frac{d^2\phi(x,y)}{dy^2} = -\frac{qN_d}{\varepsilon}, \quad \text{for } 0 \le x \le L_3, \tag{1}$$

where $\phi(x, y)$ is the potential at any point in the channel and q is the electronic charge. Solution of (1) is given by considering parabolic approximation of the potential, given by

$$\phi(x,y) = \phi_a(x) + C_1(x)y + C_2(x)y^2, \tag{2}$$

where $\phi_a(x)$ is the surface potential, $C_1(x)$ and $C_2(x)$ are arbitrary coefficients.

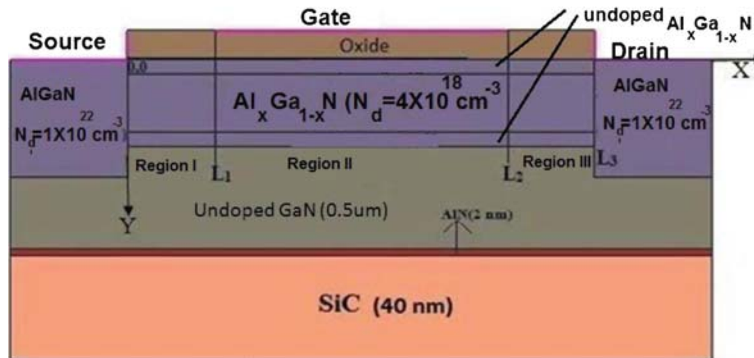

Figure 1. Two-dimensional schematic of AlGaN/GaN HEMT.

Table 1. Symbols used.

Symbols	Physical meaning/values
ε_a	Dielectric constant of AlGaN $9(m) + 9.5(1 - m)$
ε	Permittivity of AlGaN, $\varepsilon = \varepsilon_0 \varepsilon_a$
q	Charge of electron, 1.6e-19 C
σ_{po}	Polarization charge at the heterointerface
n_s^{I}	Density of 2DEG in Regions I and III
n_s^{II}	Density of 2DEG in Region II
E_{int1}, E_{int2} and E_{int3}	Vertical electric field at the heterointerface of Regions I, II and III
V_{ds}	Drain-to-source voltage
V_{bi}	Built-in voltage
V_{gs}	Gate-to-source voltage
V_{FB}	Flat band voltage
ϕ_m	Work function of the metal
$\chi_a(Al_m Ga_{1-m} N)$	Electron affinity of AlGaN given by $1.6m + 3.4(1 - m)$
$E_g(Al_m Ga_{1-m} N)$	Band gap of AlGaN given by $6.2m + 3.47(1 - m)$
D	Density of states 1e18 m^{-2} V^{-1}
V_{th}	Threshold voltage
γ_0	Experimentally determined parameters 2.12e-12
$P_{spontaneous}(Al_m Ga_{1-m} N)$	$(-0.052m - 0.029)$ C m^{-2} [21]
$P_{sponatnous}(GaN)$	-0.029 C m^{-2} [21]
$C_{13}(m)$	$5m + 103$ GPa [21]
$C_{33}(m)$	$-32m + 405$ GPa [21]
$a(m)$	$(-0.077m + 3.189)$e-10m [21]
$E_{31}(m)$	$-0.11m - 0.49$ C m^{-2} [21]
$e_{33}(m)$	$0.73m + 0.73$ C m^{-2} [21]
T	Temperature, 300 K
k	Boltzmann constant, 1.38e-23 m^2 kg s^{-2} K^{-1}

Here the channel is under three regions, where Poisson's equation will be solved simultaneously, assuming the solution as given by (2) and is

$$\phi_1(x, y) = \phi_{a1}(x) + C_1(x)y + C_2(x)y^2, \quad \text{for } 0 \le x \le L_1, \tag{3}$$

$$\phi_2(x, y) = \phi_{a2}(x) + C_3(x)y + C_4(x)y^2, \quad \text{for } L_1 \le x \le L_2, \tag{4}$$

$$\phi_3(x, y) = \phi_{a3}(x) + C_5(x)y + C_6(x)y^2, \quad \text{for } L_2 \le x \le L_3, \tag{5}$$

where $\phi_1(x, y)$, $\phi_2(x, y)$ and $\phi_3(x, y)$ are the potentials at any point under Regions I, II and III and $\phi_{a1}(x)$, $\phi_{a2}(x)$ and $\phi_{a3}(x)$ are the surface potentials under Regions I, II and III.

The Poisson's equation is solved separately for the three regions [19] using the following boundary condition:

$$\left.\frac{d\phi_1(x, y)}{dy}\right|_{y=0} = \frac{\varepsilon_{ox}}{\varepsilon_a} \frac{\phi_{a1}(x) - V_{gs1}}{t_{ox}}, \tag{6}$$

$$\left.\frac{\mathrm{d}\phi_1\,(x,y)}{\mathrm{d}y}\right|_{y=d} = \frac{-(\sigma_{\mathrm{po}} - n_{\mathrm{s}}^{\mathrm{I}})q}{\varepsilon} = -E_{\mathrm{int1}}, \tag{7}$$

$$\left.\frac{\mathrm{d}\phi_2\,(x,y)}{\mathrm{d}y}\right|_{y=0} = \frac{\varepsilon_{\mathrm{ox}}}{\varepsilon_{\mathrm{a}}}\frac{\phi_{\mathrm{a2}}(x) - V_{\mathrm{gs1}}}{t_{\mathrm{ox}}}, \tag{8}$$

$$\left.\frac{\mathrm{d}\phi_2\,(x,y)}{\mathrm{d}y}\right|_{y=d} = \frac{-(\sigma_{\mathrm{po}} - n_{\mathrm{s}}^{\mathrm{II}})q}{\varepsilon} = -E_{\mathrm{int2}}, \tag{9}$$

$$\left.\frac{\mathrm{d}\phi_3\,(x,y)}{\mathrm{d}y}\right|_{y=0} = \frac{\varepsilon_{\mathrm{ox}}}{\varepsilon_{\mathrm{a}}}\frac{\phi_{\mathrm{a3}}(x) - V_{\mathrm{gs1}}}{t_{\mathrm{ox}}}, \tag{10}$$

$$\left.\frac{\mathrm{d}\phi_3\,(x,y)}{\mathrm{d}y}\right|_{y=d} = \frac{-(\sigma_{\mathrm{po}} - n_{\mathrm{s}}^{\mathrm{I}})q}{\varepsilon} = -E_{\mathrm{int3}}, \tag{11}$$

$$\phi_{\mathrm{a1}}(x)|_{x=0} = V_{\mathrm{bi}}, \tag{12}$$

$$\phi_{\mathrm{a3}}(x)\big|_{x=L_3} = V_{\mathrm{bi}} + V_{\mathrm{ds}}. \tag{13}$$

We know

$$V_{\mathrm{gs1}} = V_{\mathrm{gs}} - V_{\mathrm{FB}}, \tag{14}$$

where $V_{\mathrm{FB}} = \phi_{\mathrm{m}} - \phi_{\mathrm{s}}$ and ϕ_{s} is the work function of $\mathrm{Al}_m\mathrm{Ga}_{1-m}\mathrm{N}$ given by $\phi_{\mathrm{s}} = \chi_{\mathrm{a}} + \left(E_{\mathrm{g}}/2\right) - \phi_{\mathrm{f}}$. ϕ_{f} is the Fermi potential given by $\phi_{\mathrm{f}} = kT/q\,\ln(N_{\mathrm{d}}/n_{\mathrm{i}})$, n_{i} being the intrinsic carrier concentration.

The total polarization of AlGaN/GaN HEMT is the sum of the spontaneous polarization and the piezoelectric polarization [21]. The total amount of polarization induced charge sheet density for $\mathrm{Al}_m\mathrm{Ga}_{1-m}\mathrm{N}$ HEMT is given as [22].

$$\begin{aligned}|\sigma_{\mathrm{po}}(m)| = {} & |P_{\mathrm{spontaneous}}(\mathrm{Al}_m\mathrm{Ga}_{1-m}\mathrm{N}) - P_{\mathrm{spontaneous}}(\mathrm{GaN}) \\ & + P_{\mathrm{piezoelectric}}(\mathrm{Al}_m\mathrm{Ga}_{1-m}\mathrm{N})|,\end{aligned} \tag{15}$$

$$\begin{aligned}P_{\mathrm{piezoelectric}}(\mathrm{Al}_m\mathrm{Ga}_{1-m}\mathrm{N}) = {} & \left(\frac{2\,(a(m) - a(0))}{a(m)}\right) \\ & \times \left(e_{31}(m) - e_{33}(m)\frac{C_{13}(m)}{C_{33}(m)}\right).\end{aligned} \tag{16}$$

In Regions I and III, 2DEG density is approximated as [17]

$$n_{\mathrm{s}}^{\mathrm{I}} = \frac{C_{\mathrm{b}}V_{\mathrm{go}}}{q}\,\frac{V_{\mathrm{go}} + V_{\mathrm{th}}[1 - \ln(\beta V_{\mathrm{go}})] - \frac{\gamma_0}{3}\left(\frac{C_{\mathrm{b}}V_{\mathrm{go}}}{q}\right)^{2/3}}{V_{\mathrm{go}} + V_{\mathrm{th}} + \frac{2\gamma_0}{3}\left(\frac{C_{\mathrm{b}}V_{\mathrm{go}}}{q}\right)^{2/3}}, \tag{17}$$

where $C_{\mathrm{b}} = \varepsilon/d$, $V_{\mathrm{go}} = V_{\mathrm{gs}} - V_{\mathrm{th}}$ and $\beta = C_{\mathrm{b}}/(qDV_{\mathrm{th}})$.

2DEG density for Region II is approximated as [19]

$$n_{\mathrm{s}}^{\mathrm{II}} = \frac{C_{\mathrm{t}}}{q}\left(V_{\mathrm{gs}} - V_{\mathrm{th}} - E_{\mathrm{F}}\right), \tag{18}$$

where $V_{\rm th}$ is given as

$$V_{\rm th} = \phi_{\rm m} - \chi - \Delta E_{\rm C} - \frac{Q_{\rm ins}}{C_{\rm ins}} - \frac{\sigma_{\rm po}}{C_{\rm t}} - \frac{qN_{\rm D}d}{C_{\rm t}} + \frac{qN_{\rm D}d^2}{2\varepsilon}. \tag{19}$$

$\Delta E_{\rm C}$ is the conduction band discontinuity, $Q_{\rm ins}$ is the interface charge of the oxide/cap layer interface and $C_{\rm t}$ is the total capacitance from gate to channel and given as $1/C_{\rm t} = 1/C_{\rm ox} + 1/C_{\rm b}$, where $C_{\rm ox}$ is the oxide capacitance.

Now, as we know surface potential and electric field at the interface of two regions are continuous, we can write boundary condition for the interface of Region I–Region II and Region II–Region III as

$$\phi_{\rm a1}(x)\big|_{x=L_1} = \phi_{\rm a2}(x)\big|_{x=L_1}, \tag{20}$$

$$\left.\frac{{\rm d}\phi_{\rm a1}(x)}{{\rm d}x}\right|_{x=L_1} = \left.\frac{{\rm d}\phi_{\rm a2}(x)}{{\rm d}x}\right|_{x=L_1}, \tag{21}$$

$$\phi_{\rm a2}(x)\Big|_{x=L_2} = \phi_{\rm a3}(x)\Big|_{x=L_2}, \tag{22}$$

$$\left.\frac{{\rm d}\phi_{\rm a2}(x)}{{\rm d}x}\right|_{x=L_2} = \left.\frac{{\rm d}\phi_{\rm a3}(x)}{{\rm d}x}\right|_{x=L_2}. \tag{23}$$

Now, constants in (3), (4) and (5) can be found from the boundary conditions (6)–(11) and substituting their values in (3), (4) and (5), we get

$$\begin{aligned}\phi_1(x,y) = {} & \phi_{\rm a1}(x) + \frac{\varepsilon_{\rm ox}}{\varepsilon_{\rm a}}\frac{\phi_{\rm a1}(x) - V_{\rm gs1}}{t_{\rm ox}}y \\ & + \left(\frac{-E_{\rm int1}}{2d} - \frac{\varepsilon_{\rm ox}}{\varepsilon_{\rm a}}\frac{\phi_{\rm a1}(x) - V_{\rm gs1}}{t_{\rm ox}(2d)}\right)y^2, \quad \text{for } 0 \le x \le L_1,\end{aligned} \tag{24}$$

$$\begin{aligned}\phi_2(x,y) = {} & \phi_{\rm a2}(x) + \frac{\varepsilon_{\rm ox}}{\varepsilon_{\rm a}}\frac{\phi_{\rm a2}(x) - V_{\rm gs1}}{t_{\rm ox}}y \\ & + \left(\frac{-E_{\rm int2}}{2d} - \frac{\varepsilon_{\rm ox}}{\varepsilon_{\rm a}}\frac{\phi_{\rm a2}(x) - V_{\rm gs1}}{t_{\rm ox}(2d)}\right)y^2, \quad \text{for } L_1 \le x \le L_2,\end{aligned} \tag{25}$$

$$\begin{aligned}\phi_3(x,y) = {} & \phi_{\rm a3}(x) + \frac{\varepsilon_{\rm ox}}{\varepsilon_a}\frac{\phi_{\rm a3}(x) - V_{\rm gs1}}{t_{\rm ox}}y \\ & + \left(\frac{-E_{\rm int3}}{2d} - \frac{\varepsilon_{\rm ox}}{\varepsilon_{\rm a}}\frac{\phi_{\rm a3}(x) - V_{\rm gs1}}{t_{\rm ox}(2d)}\right)y^2.\end{aligned} \tag{26}$$

The surface potential is obtained by substituting (24), (25) and (26) in (1). We get

$$\frac{{\rm d}^2\phi_{\rm a1}(x)}{{\rm d}x^2} - \frac{\varepsilon_{\rm ox}}{\varepsilon_{\rm a}t_{\rm ox}d}\phi_{\rm a1}(x) = \frac{\varepsilon_{\rm ox}}{\varepsilon_{\rm a}t_{\rm ox}d}\left(\begin{aligned}&\frac{-qN_{\rm d}}{\varepsilon_{\rm a}}\frac{\varepsilon_{\rm a}t_{\rm ox}d}{\varepsilon_{\rm ox}} \\ &+\frac{E_{\rm int1}}{d}\frac{\varepsilon_{\rm a}t_{\rm ox}d}{\varepsilon_{\rm ox}} - V_{\rm gs1}\end{aligned}\right), \quad \text{for } 0 \le x \le L_1, \tag{27}$$

$$\frac{{\rm d}^2\phi_{\rm a2}(x)}{{\rm d}x^2} - \frac{\varepsilon_{\rm ox}}{\varepsilon_{\rm a}t_{\rm ox}d}\phi_{\rm a2}(x) = \frac{\varepsilon_{\rm ox}}{\varepsilon_{\rm a}t_{\rm ox}d}\left(\begin{aligned}&\frac{-qN_{\rm d}}{\varepsilon_{\rm a}}\frac{\varepsilon_{\rm a}t_{\rm ox}d}{\varepsilon_{\rm ox}} \\ &+\frac{E_{\rm int2}}{d}\frac{\varepsilon_{\rm a}t_{\rm ox}d}{\varepsilon_{\rm ox}} - V_{\rm gs1}\end{aligned}\right), \quad \text{for } L_1 \le x \le L_2, \tag{28}$$

$$\frac{\mathrm{d}^2\phi_{a3}(x)}{\mathrm{d}x^2} - \frac{\varepsilon_{ox}}{\varepsilon_a t_{ox} d}\phi_{a3}(x) = \frac{\varepsilon_{ox}}{\varepsilon_a t_{ox} d}\left(\begin{array}{l}\dfrac{-qN_d}{\varepsilon_a}\dfrac{\varepsilon_a t_{ox} d}{\varepsilon_{ox}} \\ +\dfrac{E_{int3}}{d}\dfrac{\varepsilon_a t_{ox} d}{\varepsilon_{ox}} - V_{gs1}\end{array}\right), \quad \text{for } L_2 \le x \le L_3. \tag{29}$$

Solutions of (27), (28) and (29) are given as

$$\phi_{a1}(x) = A\mathrm{e}^{+k_1 x} + B\mathrm{e}^{-k_1 x} - g_1, \quad \text{for } 0 \le x \le L_1, \tag{30}$$

$$\phi_{a2}(x) = C\mathrm{e}^{+k_2 x} + D\mathrm{e}^{-k_2 x} - g_2, \quad \text{for } L_1 \le x \le L_2, \tag{31}$$

$$\phi_{a3}(x) = E\mathrm{e}^{+k_1 x} + F\mathrm{e}^{-k_1 x} - g_3, \quad \text{for } L_2 \le x \le L_3, \tag{32}$$

where

$$k_1^2 = k_2^2 = \frac{\varepsilon_{ox}}{\varepsilon_a t_{ox} d}, \quad g_1 = \left(\frac{-qN_d}{\varepsilon_a k_1^2} + \frac{E_{int1}}{\mathrm{d}k_1^2} - V_{gs1}\right),$$

$$g_2 = \left(\frac{-qN_d}{\varepsilon_a k_2^2} + \frac{E_{int2}}{\mathrm{d}k_2^2} - V_{gs1}\right)$$

and

$$g_3 = \left(\frac{-qN_d}{\varepsilon_a k_1^2} + \frac{E_{int3}}{\mathrm{d}k_1^2} - V_{gs1}\right).$$

Using boundary conditions (12), (13), (20), (21), (22) and (23), coefficients of (31)–(33) are found to be

$$A = \frac{\left\{\begin{array}{l}(V_{bi} + g_1)(X_1\mathrm{e}^{-k_1L_3} - Y_1\mathrm{e}^{k_1L_3}) + (G_2Y_1 - G_1Y_2)\mathrm{e}^{k_1L_3} \\ +(G_1X_2 - G_2X_1)\mathrm{e}^{-k_1L_3} + (V_{bi} + V_{ds} + g_3)(Y_1X_2 - X_1Y_2)\end{array}\right\}}{(X_1 + X_2)\mathrm{e}^{-k_1L_3} - (Y_1 + Y_2)\mathrm{e}^{+k_1L_3}}, \tag{33}$$

$$B = \frac{\left\{\begin{array}{l}(V_{bi} + g_1)(X_2\mathrm{e}^{-k_1L_3} - Y_2\mathrm{e}^{k_1L_3}) + (G_1Y_2 - G_2Y_1)\mathrm{e}^{k_1L_3} \\ +(G_2X_1 - G_1X_2)\mathrm{e}^{-k_1L_3} + (V_{bi} + V_{ds} + g_3)(Y_2X_1 - X_2Y_1)\end{array}\right\}}{(X_1 + X_2)\mathrm{e}^{-k_1L_3} - (Y_1 + Y_2)\mathrm{e}^{+k_1L_3}}, \tag{34}$$

$$C = \frac{\left\{\begin{array}{l}2\mathrm{e}^{-(k_2L_2+k_1L_3)}(k_1\cosh(k_1L_2) \\ +k_2\sinh(k_1L_2))((V_{bi} + g_1) - (G_1 + G_2)) \\ +(V_{bi} + V_{ds} + g_3)(\mathrm{e}^{-k_1L_2}(k_2 - k_1)(X_1 + X_2) \\ -\mathrm{e}^{k_1L_2}(k_1 + k_2)(Y_1 + Y_2))\end{array}\right\}}{2k_2((X_1 + X_2)\mathrm{e}^{-k_1L_3} - (Y_1 + Y_2)\mathrm{e}^{+k_1L_3})} + \frac{1}{2}\mathrm{e}^{-k_2L_2}(g_2 - g_3), \tag{35}$$

$$D = \frac{\left\{\begin{array}{l}2\mathrm{e}^{-(k_1L_3-k_2L_2)}(k_2\sinh(k_1L_2) \\ -k_1\cosh(k_1L_2))((V_{bi} + g_1) - (G_1 + G_2)) \\ +(V_{bi} + V_{ds} + g_3)(\mathrm{e}^{-k_1L_2}(k_2 + k_1)(X_1 + X_2) \\ -\mathrm{e}^{k_1L_2}(k_2 - k_1)(Y_1 + Y_2))\end{array}\right\}}{2k_2((X_1 + X_2)\mathrm{e}^{-k_1L_3} - (Y_1 + Y_2)\mathrm{e}^{+k_1L_3})} + \frac{1}{2}\mathrm{e}^{+k_2L_2}(g_2 - g_3), \tag{36}$$

$$E=\frac{\left\{\begin{array}{l}((V_{\rm bi}+g_1)-(G_1+G_2))\mathrm{e}^{-k_1L_3}\\-(V_{\rm bi}+V_{\rm ds}+g_3)(Y_1+Y_2)\end{array}\right\}}{(X_1+X_2)\mathrm{e}^{-k_1L_3}-(Y_1+Y_2)\mathrm{e}^{+k_1L_3}}, \tag{37}$$

$$F=\frac{\left\{\begin{array}{l}(V_{\rm bi}+V_{\rm ds}+g_3)(X_1+X_2)\\-((V_{\rm bi}+g_1)-(G_1+G_2))\mathrm{e}^{k_1L_3}\end{array}\right\}}{(X_1+X_2)\mathrm{e}^{-k_1L_3}-(Y_1+Y_2)\mathrm{e}^{+k_1L_3}}, \tag{38}$$

where

$$X_1=\frac{\mathrm{e}^{-k_1(L_1-L_2)}(\mathrm{e}^{k_2(L_1-L_2)}(k_1+k_2)^2-\mathrm{e}^{-k_2(L_1-L_2)}(k_1^2-k_2^2))}{4k_1k_2},$$

$$X_2=\frac{\mathrm{e}^{k_1(L_1+L_2)}(k_1^2-k_2^2)\sinh(k_2(L_1-L_2))}{2k_1k_2},$$

$$Y_1=\frac{\mathrm{e}^{-k_1(L_1+L_2)}(k_2^2-k_1^2)\sinh(k_2(L_1-L_2))}{2k_1k_2},$$

$$Y_2=\frac{\mathrm{e}^{k_1(L_1-L_2)}(\mathrm{e}^{-k_2(L_1-L_2)}(k_1+k_2)^2-\mathrm{e}^{k_2(L_1-L_2)}(k_1^2-k_2^2))}{4k_1k_2},$$

$$G_1=\frac{\left\{\begin{array}{l}\mathrm{e}^{-k_1L_1}((g_2-g_3)(k_1\cosh(k_2(L_1-L_2))\\+k_2\sinh(k_2(L_1-L_2)))+k_1(g_1-g_2))\end{array}\right\}}{2k_1}$$

and

$$G_2=\frac{\left\{\begin{array}{l}\mathrm{e}^{k_1L_1}((g_2-g_3)(k_1\cosh(k_2(L_1-L_2))\\-k_2\sinh(k_2(L_1-L_2)))+k_1(g_1-g_2))\end{array}\right\}}{2k_1}.$$

3.1 *Surface potential*

Surface potential for channel length $x=0$ to $x=L_3$ can be given as

$$\phi_{\rm a}(x)=\phi_{\rm a1}(x)+\phi_{\rm a2}(x)+\phi_{\rm a3}(x), \tag{39}$$

where $\phi_{\rm a1}(x)$, $\phi_{\rm a2}(x)$ and $\phi_{\rm a3}(x)$ are given by (31), (32) and (33).

3.2 *Channel potential*

Channel potential for channel length $x=0$ to $x=L_3$ can be determined by substituting $y=d$ in (24), (25) and (26).

Therefore, the channel potential is given by

$$\phi(x,d)=\phi_1(x,d)+\phi_2(x,d)+\phi_3(x,d), \tag{40}$$

where

$$\phi_1(x,d)=\phi_{\rm a1}(x)+\frac{\varepsilon_{\rm ox}}{\varepsilon_{\rm a}}\frac{\phi_{\rm a1}(x)-V_{\rm gs1}}{2t_{\rm ox}}d+\frac{-E_{\rm int1}d}{2},\quad \text{for } 0\le x\le L_1, \tag{41}$$

$$\phi_2(x,d) = \phi_{a2}(x) + \frac{\varepsilon_{ox}}{\varepsilon_a}\frac{\phi_{a2}(x) - V_{gs1}}{2t_{ox}}d + \frac{-E_{int2}d}{2}, \quad \text{for } L_1 \le x \le L_2, \tag{42}$$

$$\phi_3(x,d) = \phi_{a3}(x) + \frac{\varepsilon_{ox}}{\varepsilon_a}\frac{\phi_{a3}(x) - V_{gs1}}{2t_{ox}}d + \frac{-E_{int3}d}{2}, \quad \text{for } L_2 \le x \le L_3. \tag{43}$$

3.3 *Electric field*

In this paper, we have assumed vertical electric field at the heterointerface to be uniform and it has been used as boundary condition.

Lateral electric field, which is responsible for current drive in the channel, can be expressed as

$$E_{fx} = -\frac{\mathrm{d}\phi(x)}{\mathrm{d}x}. \tag{44}$$

Now, electric field along the channel length $x = 0$ to $x = L_3$ can be obtained from (41), (42), (43) and (44).

Electric field along the channel can be expressed as

$$E_{fx} = E_{fx1} + E_{fx2} + E_{fx3}, \tag{45}$$

where

$$E_{fx1} = -\left(1 + \frac{\varepsilon_{ox}d}{2\varepsilon_{ox}t_{ox}}\right)\frac{\mathrm{d}\phi_1(x)}{\mathrm{d}x}, \quad \text{for } 0 \le x \le L_1, \tag{46}$$

$$E_{fx2} = -\left(1 + \frac{\varepsilon_{ox}d}{2\varepsilon_{ox}t_{ox}}\right)\frac{\mathrm{d}\phi_2(x)}{\mathrm{d}x}, \quad \text{for } L_1 \le x \le L_2, \tag{47}$$

$$E_{fx3} = -\left(1 + \frac{\varepsilon_{ox}d}{2\varepsilon_{ox}t_{ox}}\right)\frac{\mathrm{d}\phi_3(x)}{\mathrm{d}x}, \quad \text{for } L_2 \le x \le L_3. \tag{48}$$

The drain current in channel [24]

$$I_{ds}(x) = qwn_s(x)V(x), \tag{49}$$

where q is the electron charge, w is the gate width and $V(x)$ is the carrier velocity.

$$V(x) = \frac{\mu E(x)}{1 + (E(x)/E_c)}, \quad \text{for } E < E_c, \tag{50}$$

$$= V_{sat}, \quad \text{for } E > E_c. \tag{51}$$

In linear region, we have

$$V(x) = \frac{\mu E(x)}{1 + (E(x)/E_c)} = \frac{\mu E(x)}{1 + (\mu E(x)/V_{sat})} = \frac{\mu V_{sat} E(x)}{V_{sat} + \mu E(x)}, \tag{52}$$

where V_{sat} is the saturation velocity and μ is the mobility of the carriers.

Putting the value of $n_s(x)$ from (18)

$$I_{ds}(x) = qwn_s(x)\frac{\mu E(x)V_{sat}}{V_{sat}+\mu E(x)},$$

$$= qW\left[\frac{C_t}{q}(V_{gs}-V_{th}-E_F)\right]\frac{\mu E(x)V_{sat}}{V_{sat}+\mu E(x)}, \tag{53}$$

where

$$C_t = \frac{C_{ox}C_b}{C_{ox}+C_b},$$

C_{ox} and C_b are oxide and bulk capacitances.

In saturation region,

$$V(x) = V_{sat}, \quad I_{ds}(x) = qwn_s(x)V_{sat}. \tag{54}$$

Putting $n_s(x)$ we get

$$I_{ds}(x) = qw\left[\frac{C_t}{q}\left(V_{gs}-V_{th}-E_F\right)\right]V_{sat}. \tag{55}$$

4. Results and discussions

The mathematical model developed for potential and electric field has been compared with simulated structure. The Sentaurus TCAD [23] is used to simulate the structure. The physical models used for the simulation are: hydrodynamic model for determining carrier temperature, Fermi–Dirac statistics for high doping concentration, mobility model used are eHighfieldsaturation and doping dependence, SRH and Auger models have been used as recombination models and band-gap narrowing effect has been disabled. Polarization charges have been included in the heterointerface and interface charges at oxide/cap layer interface. Traps have been included for AlGaN and GaN layers. Our mathematical model is compared with simulated structure for different gate lengths, mole fractions and drain voltages. Our model device has mole fraction less than 0.4 because HEMT devices with mole fractions greater than 0.4 are not of high quality [21].

In figure 2 variation of surface potential for different gate lengths is shown. It is observed that surface potential is symmetrical about the middle of the channel, and it decreases with increase in gate length, where at the middle, minimum channel potential decreases with increase in gate length and it shows the presence of short channel effect. Moreover, the potential minimum increases with the decrease in gate length, which result in reduced barrier and signify the presence of barrier lowering effect.

Variations of surface potential for different mole fractions are shown in figure 3 which depicts that simulated results completely matched with modelled results. Variations of surface potential for different drain voltages can be observed in figure 4. Here, it can be seen that at drain side, with increase in drain voltage, surface potential increases due to increase of reverse bias near the drain. The modelled results are in close agreement with the simulated structure except near the source and the drain because of the finite values in boundary conditions. In figure 5, variations of channel potential for different gate

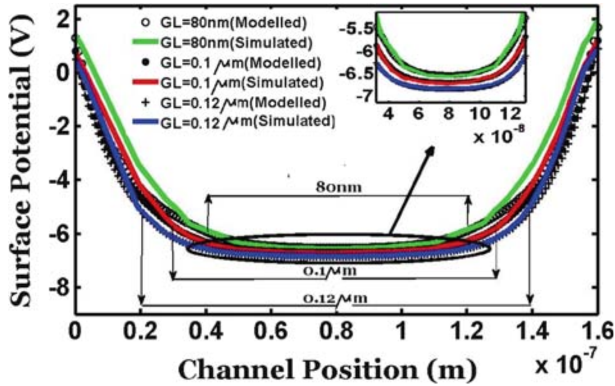

Figure 2. Plot of surface potential vs. channel position for different gate lengths (GL) of 80 nm, 0.1 μm and 0.12 μm for fixed drain voltage = 0.4 V, mole fraction = 0.2 and gate voltage = −6.2 V.

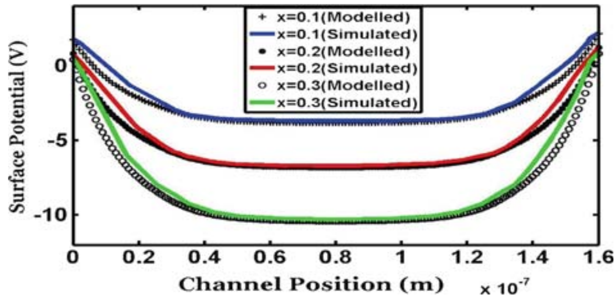

Figure 3. Plot of surface potential vs. channel position for mole fractions = 0.1, 0.2 and 0.3 for 100 nm gate length at a constant drain voltage of 0.4 V. Gate voltage = −5.3, −6.2 and −10.4 V for 0.1, 0.2 and 0.3 mole fractions.

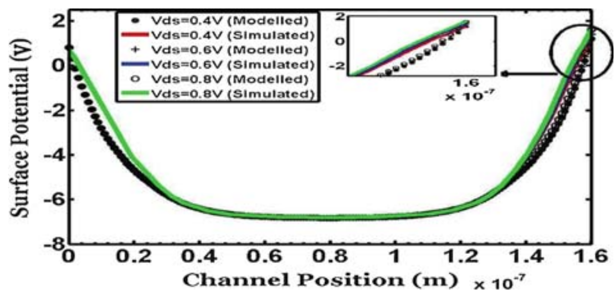

Figure 4. Plot of surface potential vs. channel position for drain voltage = 0.4, 0.6 and 0.8 V for gate length = 100 nm, mole fraction = 0.2 and gate voltage = −6.2 V.

lengths are shown and it is observed that as gate length increases, the potential minimum decreases in a way similar to the drain current. It is observed that potential is less in source side for all gate lengths. This signifies the presence of short channel effect. Modelled results closely match with the simulation. Figure 6 shows variation of channel potential

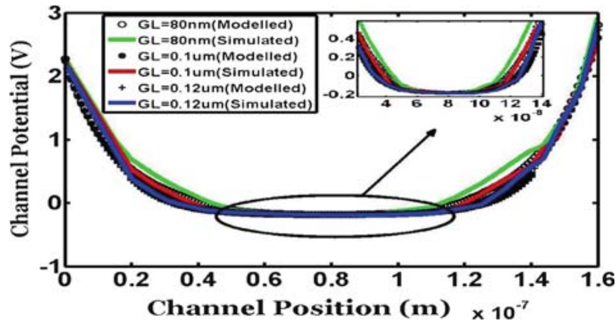

Figure 5. Plot of channel potential vs. channel position for three different gate lengths (GL) of 80 nm, 0.1 μm and 0.12 μm for a constant drain voltage of 0.4 V at mole fraction = 0.2 and gate voltage = −6.2 V.

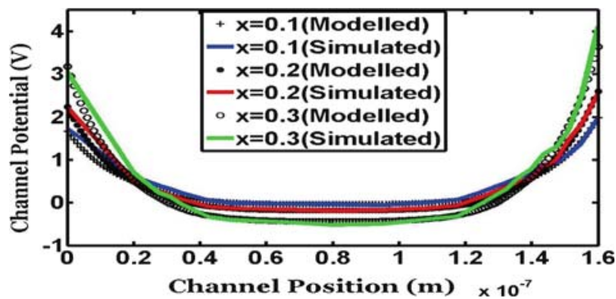

Figure 6. Plot of channel potential vs. channel position for different mole fractions of 0.1, 0.2 and 0.3 for 100 nm gate length at a constant drain voltage of 0.4 V. Gate voltage = −5.3, −6.2 and −10.4 V for mole fraction = 0.1, 0.2 and 0.3.

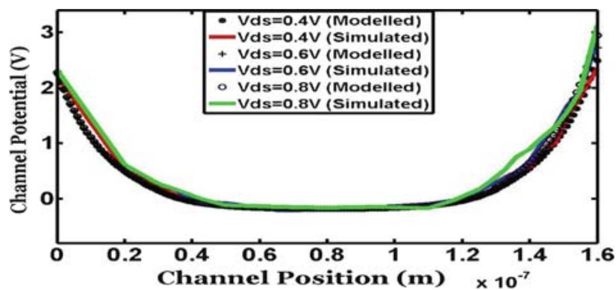

Figure 7. Plot of channel potential vs. channel position for different drain voltages of $V_{\rm ds}$ = 0.4, 0.6 and 0.8 V at gate voltage = −6.2 V, gate length = 100 nm and mole fraction = 0.2.

for different mole fractions, where, we have observed simulation results closely agree with the model result.

Variations of channel potential for different drain voltages are shown in figure 7 and it was observed that with increase of drain voltage, channel potential increases leading to increase in current. In figure 8, variations of electric field across the channel for different

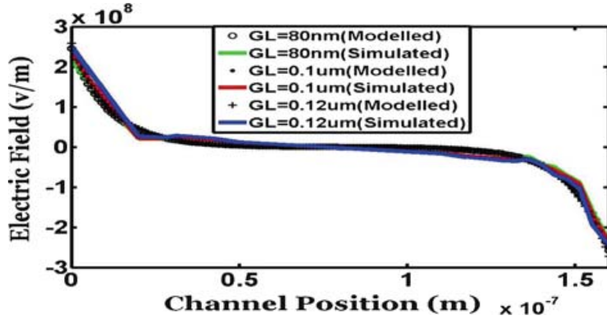

Figure 8. Plot of electric field vs. channel position for different gate lengths (GL) of 80 nm, 0.1 μm and 0.12 μm for a constant drain voltage of 0.4 V at mole fraction = 0.2 and gate voltage = −6.2 V.

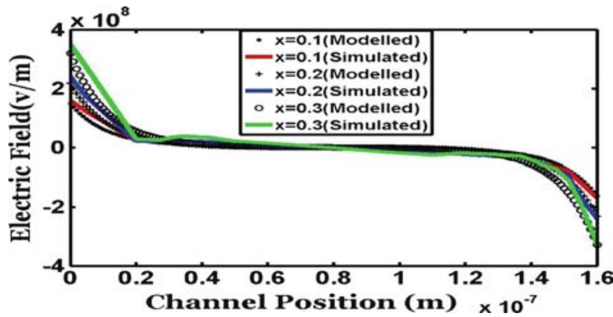

Figure 9. Plot of electric field vs. channel position for different mole fractions of 0.1, 0.2 and 0.3 for 100 nm gate length at a constant drain voltage of 0.4 V. Gate voltage = −5.3, −6.2 and −10.4 V for mole fraction = 0.1, 0.2 and 0.3.

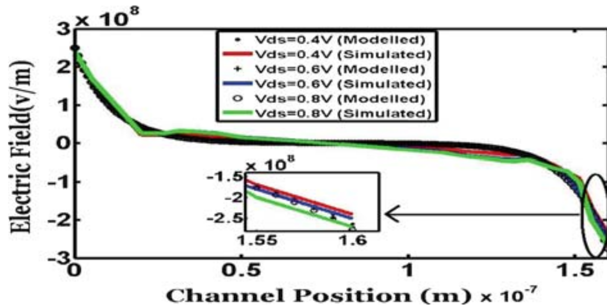

Figure 10. Plot of electric field vs. channel position for a fixed gate length of 100 nm at three different drain voltages of 0.4, 0.6 and 0.8 V at gate voltage = −6.2 V and mole fraction = 0.2.

gate lengths are shown, and it is found that simulated results closely match with the modelled results except near the source and the drain end which might be due to the finite values used in boundary conditions.

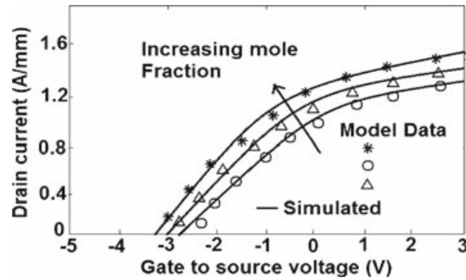

Figure 11. Drain current vs. gate to source voltage graph for mole fraction = 0.1, 0.2 and 0.3.

Figure 9 shows variation of lateral electric field with different mole fractions. It is observed that simulated results match closely with the modelled results. Variations of electric field across the channel for different drain voltages are shown in figure 10 and it can be observed that in the drain side, lateral electric field increases with drain voltage in a similar way as channel potential, shown in figure 7. Figure 11 predicts the drain current of the proposed device for varying mole fractions. The simulated data are compared with the model values obtained from analytical expressions given in (53) and (55). The simulated data closely approach the analytical values.

5. Conclusion

The analytical model presented in this paper for surface potential, channel potential, electric field and drain current is found to be valid for AlGaN/GaN HEMT with high-K gate dielectric without using any fitting parameter and serves efficiently for HEMT with gate dielectric.

References

[1] U K Mishra, Y F Wu, B P Keller, S Keller and S P Denbaars, *IEEE Trans. Microwave Theory Tech.* **46(6)**, 756 (1998)
[2] U K Mishra, P Parikh and Y F Wu, *Proc. IEEE* (2002) pp. 1022–1031
[3] M S Shur, R Gaska, A Khan and G Simin, Wide band gap electronic devices, *Proc. 4th IEEE Int. Caracas Conf. on Devices, Circuits and Systems* (Aruba, 2002), pp. D051-1–D051-8
[4] A V Vertiatchikh and L F Eastman, *IEEE Electron Device Lett.* **24**(**9**), 535 (2003)
[5] G Meneghesso, G Verzellesi, F Danesin, F Rampazzo, F Zanon, A Tazzoli, M Meneghini and E Zanoni, *IEEE Trans. Device Mater. Rel.* **8**(**2**), 332 (2009)
[6] V Adivarahan, M Gaeyski, W H Sun, H Fatima, A Koudymov, S Saygi, J Yang, M A Khan, A Tarakji, M S Shur and R Gaska, *IEEE Electron Device Lett.* **24**(**9**), 541 (2003)
[7] C Liu, E F Chor and L S Tan, *Appl. Phys. Lett.* **88**(**17**), 173504-1173504-3 (2006)
[8] P D Ye, B Yeng, K K Ng, J Bude, G D Wilk, S Halder and J Hwang, *Appl. Phys. Lett.* **86**(**6**), 063501-063501-3 (2005)
[9] A Koudymov, M S Shur, G Simin, K Chu, P C Chao, C Lee, J Jimenez and A Balisteri, *IEEE Trans. Electron Devices* **55**(**3**), 712 (2008)

[10] K Lee, M Shur, T J Drummonod and H Morkoc, *IEEE Trans. Electron Devices* **30**(**3**), 207 (1983)
[11] X Cheng, M Li and Y Wang, *IEEE Trans. Electron Devices* **56**(**1**), 261 (2008)
[12] S P Kumar, A Agarwal, R Chaujar, S Kabra, M Gupta and R S Gupta, *Microelectron. J.* **38**, 1013 (2007)
[13] J Si, J Wei, W Chen and B Zhang, *IEEE Trans. Electron Devices* **60**(**10**), 3223 (2013)
[14] X Cheng and Y Wang, *IEEE Trans. Electron Devices* **58**(**2**), 448 (2011)
[15] S Khandelwal, Y S Chauhan and T A Fjeldly, *IEEE Trans. Electron Devices* **59**(**10**), 2856 (2012)
[16] S P Kumar, A Agarwal, R Chaujar, M Gupta and R S Gupta, *Superlattices and Microstructures* **44**, 37 (2008)
[17] S Khandelwal, N Goyal and T A Fjeldly, *IEEE Trans. Electron Devices* **58**(**10**), 3622 (2011)
[18] W Jie, S Lingling, L Jun and Z Mingzhu, *J. Semicond.* **34**(**9**), 094002-1–094002-4 (2013)
[19] L Shenghui, D Jiangfeng, L Qian, Y Qi, Z Wei, X Jianxin and Y Mohua, *J. Semicond.* **31**(**9**), 094004-1 (2010)
[20] L Shen, D Buttari, S Heikman, A Chini, R Coffie, L McCarthy, A Chakraborty, S Keller, S P DenBaars and U K Mishra, in: *62nd DRC Device Research Conf.*, (2004) pp. 39–40
[21] O Ambacher, B Foutz, J Smart, J R Shealy, O Ambacher, J Smart, J R Shealy, N G Weimann, K Chu, M Murphy, W J Schaff, L F Eastman, R Dimitrov, L Wittmer, M Stutzmann, W Rieger and J Hilsenbeck, *J. Appl. Phys.* **85**(**6**), 3222 (1999)
[22] Rashmi, A Kranti, S Haldar and R S Gupta, *Solid-State Electron.* **46**, 621 (2002)
[23] Sentaurus Device User Guide, Synopsys, Inc. (2011)
[24] R Aggarwal, A Agrawal, M Gupta and R S Gupta, *Microwave Opt. Technol. Lett.* **50**, 331 (2008)